

## A single-photon source based on a single $\text{Ca}^+$ ion

Christian Maurer, Christoph Becher<sup>1</sup>, Carlos Russo,  
Jürgen Eschner<sup>2</sup> and Rainer Blatt<sup>3</sup>

Institut für Experimentalphysik, Universität Innsbruck, Technikerstraße 25,  
A-6020 Innsbruck, Austria

E-mail: [christoph.becher@uibk.ac.at](mailto:christoph.becher@uibk.ac.at)

*New Journal of Physics* **6** (2004) 94

Received 23 February 2004

Published 29 July 2004

Online at <http://www.njp.org/>

doi:10.1088/1367-2630/6/1/094

**Abstract.** We propose a deterministic source of single photons based on the vacuum-stimulated Raman transition of a single  $\text{Ca}^+$  ion trapped inside a high finesse cavity. Assuming realistic experimental parameters, the efficiency of photon emission into the cavity mode reaches 95%.

<sup>1</sup> Author to whom any correspondence should be addressed.

<sup>2</sup> Present address: Institut for Photonic Sciences (ICFO), C/ Jordi Girona, 29, 08034-Barcelona, Spain.

<sup>3</sup> Also with: Institut für Quantenoptik und Quanteninformation, Österreichische Akademie der Wissenschaften, Technikerstraße 25, A-6020 Innsbruck, Austria.

**Contents**

<b>1. Introduction</b>	<b>2</b>
<b>2. Population transfer in three-level systems</b>	<b>3</b>
2.1. Raman process . . . . .	3
2.2. Adiabatic process . . . . .	4
<b>3. Experimental atom–cavity system</b>	<b>5</b>
3.1. Calcium ion and ion trap . . . . .	5
3.2. Optical cavity and coupling parameters . . . . .	6
<b>4. Theoretical model</b>	<b>6</b>
<b>5. Single-photon emission: theoretical results</b>	<b>8</b>
5.1. Raman process . . . . .	8
5.2. Adiabatic process . . . . .	10
5.3. Comparison of adiabatic and Raman process . . . . .	12
<b>6. Intensity correlation</b>	<b>15</b>
<b>7. Summary and discussion</b>	<b>16</b>
<b>Acknowledgments</b>	<b>18</b>
<b>References</b>	<b>18</b>

**1. Introduction**

The deterministic generation of single photons in a well-defined spatial and spectral mode of the radiation field represents the ultimate control of the light emission process. Many applications in the emerging field of quantum information science [1] require such a deterministic source of single photons. Most of the proposed and/or demonstrated schemes for single-photon generation rely on the spontaneous emission of an excited emitter with the inherent disadvantage of spatial and spectral uncertainties, even if coupled to a cavity. Such triggered single-photon emitters have been realized with molecules [2, 3], quantum well p–i–n hetero-junctions [4], colour centres [5, 6] and semiconductor quantum dots [7, 8]. On the other hand, proposed schemes based on stimulated (Raman) transitions of an emitter coupled to a cavity mode offer the advantage of photon emission into a single spatial and spectral mode of the radiation field [9]–[11]. Stimulated single-photon emission has been demonstrated employing neutral atoms falling through a high finesse optical cavity [12]. However, as the atoms do not couple stationary to the cavity field there is a large uncertainty in the number of photons emitted by each atom. In addition, the atoms arrive at random times at the cavity mode and the number of atoms coupled to the mode fluctuates with Poissonian statistics. Very recently, the deterministic generation of single photons with high efficiency from one atom trapped inside a cavity has been reported [13].

Photon emission schemes based on stimulated Raman transitions also offer the possibility to transfer quantum information stored in internal atomic states to a light field by coupling to a cavity mode [14]. The interconnection of multiple atom–cavity systems via photonic channels then allows for transport of quantum information within distributed quantum networks [15]. Realization of a quantum network requires an interface between atoms as static quantum bits and photons as moving quantum bits. Such an interface could be based on the deterministic coupling of a single atom or ion to a high finesse optical cavity [16, 17], which

requires the ability to precisely and stationary place the atom at a fixed position within the cavity field.

There have been recent achievements in transporting, temporarily trapping and localizing neutral atoms inside high finesse optical cavities [18]–[20] which partially have resulted in deterministic single-photon emission [13]. On the other hand, trapped and laser-cooled ions are ideally suited systems for the realization of deterministic single-photon sources and atom–photon interfaces. A trapped ion’s motional wavepacket is confined to a region much smaller than the optical wavelength  $\lambda$  (to approximately  $\lambda/50$ ) and its position within a cavity standing wave (SW) field can be controlled with a precision of up to 7 nm [17]. In addition, by applying external laser fields, one can fully control the motional and internal quantum state of a trapped ion [21, 22].

In the present paper, we study the implementation of a deterministic source of single photons based on the vacuum-stimulated Raman transition of a single  $\text{Ca}^+$  ion trapped inside a high finesse cavity. Our proposal combines the advantages of stimulated Raman emission schemes and laser-cooled trapped ions, stationary coupled to the mode of a high finesse optical cavity. The paper is organized as follows. In section 2, we review population transfer schemes in three-level systems and compare Raman and adiabatic processes. In section 3, we present the physical system consisting of the single  $^{40}\text{Ca}^+$  ion and the high finesse optical cavity. In sections 4 and 5, we describe the theoretical model based on realistic parameters and results for the two types of population transfer processes. The intensity correlation function for a train of single photons produced by Raman transfer is calculated in section 6.

## 2. Population transfer in three-level systems

In a three-level  $\Lambda$ -system, as depicted in figure 1, with two ground states  $|1\rangle$  and  $|3\rangle$ , one can, in principle, coherently transfer the whole population from one ground state to the other. In the following, we review two possible processes fulfilling this condition. The general scheme investigated is a  $\Lambda$ -system initially prepared in state  $|1\rangle$  and emitting a single photon upon transition between states  $|2\rangle$  and  $|3\rangle$ .

### 2.1. Raman process

If the lasers are far detuned from atomic resonance, i.e.  $(\Delta_1, \Delta_3) \gg (\Omega_{12}, \Omega_{23}, \Gamma_{21}, \Gamma_{23})$  and the difference of the detunings is not too large ( $|\Delta_1 - \Delta_3| \ll (\Delta_1, \Delta_3)$ ) the population of level  $|2\rangle$  becomes very small and one can eliminate this level adiabatically. In this regime an effective two-level system is obtained. The population transfer from level  $|1\rangle$  to level  $|3\rangle$  can be calculated from the solutions of a two-level system with an effective Rabi frequency  $\Omega_{eff} = \Omega_{12}\Omega_{23}/(2\Delta_1)$  [23]. The effective spontaneous emission rate from level  $|2\rangle$  can then be calculated as  $\Gamma_{eff} = \Gamma\Omega_{12}^2/(4\Delta_1^2)$  with  $\Gamma = \Gamma_{21} + \Gamma_{23}$  being the total emission rate from level  $|2\rangle$ . The interaction of the radiation field with the atom induces an AC-Stark splitting of the atomic levels. For the case  $\Omega_{12} \gg \Omega_{23} \gg \Gamma$  the splitting is  $\lambda_{\pm} = \frac{1}{2}(\Delta_1 \pm \sqrt{\Delta_1^2 + \Omega_{12}^2})$ .<sup>4</sup> If the second laser is resonant with the level shifted by the AC-Stark effect ( $\Delta_3 = \lambda_+$ ), a two-photon resonance condition is achieved. In this case, it is possible to obtain a complete coherent population transfer between levels  $|1\rangle$  and  $|3\rangle$ . The effective Rabi frequency for the transfer is proportional to  $\Omega_{12}/\Delta_1$

<sup>4</sup> Note that the theoretical model presented in section 4 is not restricted to this case.

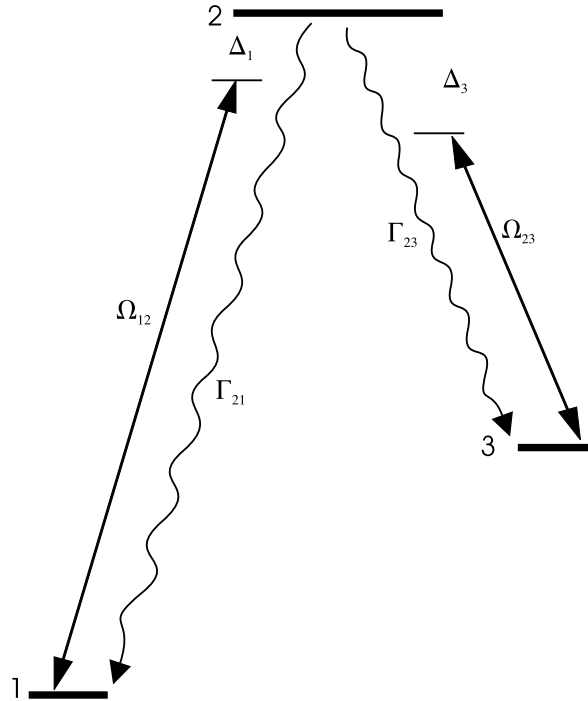


**Figure 1.** Level scheme for a three-level  $\Lambda$ -configuration.  $\Omega_{12}$  and  $\Omega_{23}$  denote coupling of levels  $|1\rangle$ – $|2\rangle$  and  $|2\rangle$ – $|3\rangle$  by external fields with detuning  $\Delta_1$  and  $\Delta_3$ , respectively. Level  $|2\rangle$  decays with a rate of  $\Gamma_{21}$  and  $\Gamma_{23}$  into states  $|1\rangle$  and  $|3\rangle$ , respectively.

whereas the emission rate is proportional to  $(\Omega_{12}/\Delta_1)^2$ . It is thus always possible to achieve an effective Rabi frequency larger than the spontaneous emission rate,  $\Omega_{eff} > \Gamma_{eff}$ , if the detuning is large enough, i.e. if the condition  $\Omega_{12}/\Delta_1 < (2\Omega_{23})/\Gamma$  is fulfilled. This is also the case for a small Rabi frequency  $\Omega_{23}$  and a large emission rate  $\Gamma$ .

## 2.2. Adiabatic process

Another process to achieve a population transfer with small residual population in level  $|2\rangle$  is the technique of stimulated Raman adiabatic passage (STIRAP) [24]. Using the same notation as in the previous section, the Hamiltonian of a three-level system can be written as

$$H = \frac{\hbar}{2} \begin{pmatrix} 2\Delta_1 & \Omega_{12}^* & 0 \\ \Omega_{12} & 0 & \Omega_{23}^* \\ 0 & \Omega_{23} & 2\Delta_3 \end{pmatrix} \quad (1)$$

If both lasers have the same detuning,  $\Delta_1 = \Delta_3$ , one obtains the following eigenstates:

$$\begin{aligned} |a^+\rangle &= \sin\theta \sin\phi |1\rangle + \cos\phi |2\rangle + \cos\theta \sin\phi |3\rangle, \\ |a^0\rangle &= \cos\theta |1\rangle - \sin\theta |3\rangle, \\ |a^-\rangle &= \sin\theta \cos\phi |1\rangle - \sin\phi |2\rangle + \cos\theta \cos\phi |3\rangle. \end{aligned} \quad (2)$$

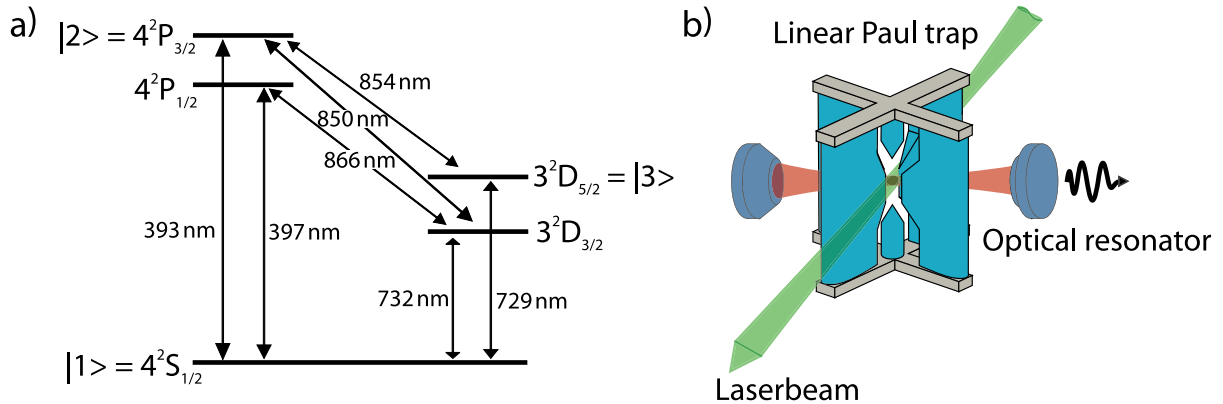


**Figure 2.** Relevant levels of the  $^{40}\text{Ca}^+$  ion (a) and sketch of the linear ion trap cavity system (b).

Here, the mixing angle  $\theta$  is defined as  $\tan \theta = \Omega_{12}/\Omega_{23}$  (the angle  $\phi$  is not important for the following discussion [11, 24]). The energies of the above eigenstates are ( $\Delta_1 = \Delta_3$ ):  $\omega^\pm = \frac{1}{2}(\Delta_1 \pm \sqrt{\Delta_1^2 + \Omega_{12}^2 + \Omega_{23}^2})$  and  $\omega^0 = \Delta_1$ , respectively. The eigenstate  $|a^0\rangle$  is a dark state with regard to emission from level  $|2\rangle$ . Population transfer from level  $|1\rangle$  to  $|3\rangle$  can be achieved by slowly varying the mixing angle from  $\theta = 0$  to  $\theta = \pi/2$ , i.e. by varying the laser intensities. The alteration of the laser intensities has to occur slowly to prevent the system from occupying state  $|2\rangle$ . A measure for the non-adiabatic coupling between the dark state and states  $|a^\pm\rangle$  is given by the matrix element  $|\langle a^\pm | \dot{a}^0 \rangle|$ . The loss of the dark state is small when the matrix element is small compared with the splitting of the energy eigenvalues  $|\langle a^\pm | \dot{a}^0 \rangle| \ll |\omega^\pm - \omega^0|$ , which yields  $|\dot{\theta}| \ll |\omega^\pm - \omega^0|$  as a criterion for the condition of adiabaticity [11, 25].  $|\dot{\theta}|$  depends on the temporal variation of  $\Omega_{12}$  and  $\Omega_{23}$  and is discussed for our scheme in section 5.2.

### 3. Experimental atom–cavity system

#### 3.1. Calcium ion and ion trap

Figure 2 shows the relevant energy levels of the  $^{40}\text{Ca}^+$  ion. The three-level system considered here is spanned by the  $S_{1/2}$ – $P_{3/2}$  transition (393 nm), driven by an external laser field, and the levels  $P_{3/2}$ – $D_{5/2}$  which are coupled by a cavity mode (854 nm). The lifetime of the  $D_{5/2}$  state is 1.16 s, which can be considered as stable compared with the time scale of the population transfer process of 50  $\mu\text{s}$ . The lifetime of the  $P_{3/2}$  state is 7.4 ns, and the branching ratios from  $P_{3/2}$  to  $S_{1/2}$ ,  $D_{5/2}$  and  $D_{3/2}$  are 1;(1/17.6);(1/150.8), respectively [26]. The  $S_{1/2}$ – $P_{1/2}$  transition at 397 nm is used to Doppler-cool the ion. Lasers at 866 and 854 nm are required to prevent shelving of the ion in one of the D states. In the proposed experiments, we use the following stabilized laser sources: two cavity-locked diode lasers at 866 and 854 nm and two Ti:Sa lasers at 786 nm (<1 kHz linewidth) and 794 nm (<300 kHz linewidth), both resonantly frequency-doubled to obtain light at 393 and 397 nm, respectively. For coherent manipulation on the  $S_{1/2}$ – $D_{5/2}$  transition, a Ti:Sa laser at 729 nm (<1 kHz linewidth) is available. A magnetic field of 3 G splits the energy levels into Zeeman components. For dipole transitions between S, P and D states, the matrix elements are largest for the outermost Zeeman substates. Therefore, we choose the states  $|S_{1/2}, m_j = -1/2\rangle$ ,  $|P_{3/2}, m_j = -3/2\rangle$  and  $|D_{5/2}, m_j = -5/2\rangle$  as  $\Lambda$ -system.

For the experiments, the  $^{40}\text{Ca}^+$  ion will be stored in the harmonic potential of a linear Paul trap [27]. The trap is made of four blades for radial confinement with a spacing of 1 mm and two tips for axial confinement with a spacing of 5 mm (see figure 2).

### 3.2. Optical cavity and coupling parameters

The transition from the  $P_{3/2}$  state to the  $D_{5/2}$  state is driven by the vacuum field of an optical resonator placed around the ion trap (see figure 2). The cavity mirrors are mounted on piezo translators so that the ion can be placed at an arbitrary position within the cavity standing wave field.

The parameter  $g$  for the coupling of a two-level system and a cavity mode can be calculated [28] for the  $|P_{3/2}, m_j = -3/2\rangle$  to  $|D_{5/2}, m_j = -5/2\rangle$  transition as

$$g = \sqrt{\frac{2c\gamma_{\perp}\lambda^2}{\pi^2 L\omega_0^2}}, \quad (3)$$

where  $L$  denotes the cavity length,  $\omega_0$  the waist radius and  $2\gamma_{\perp} = \gamma_{\parallel} = \Gamma_{23}$  the spontaneous decay rate on the  $|P_{3/2}, m_j = -3/2\rangle$  to  $|D_{5/2}, m_j = -5/2\rangle$  transition. Note that the vacuum-Rabi frequency for the above transition is  $\Omega_{23} = 2g$ . Equation 3 shows that the coupling strength  $g$  can be increased by decreasing the mode volume  $L\omega_0^2$ . However, the minimum distance of the two mirrors is limited by the extension of the ion trap. Here, a near concentric cavity will give the smallest mode cross-section for a given cavity length. In the experiment, the cavity mirrors have a radius of curvature of 10 mm and are placed at a distance of 19.95 mm, giving rise to a waist radius of  $\omega_0 = 11.65 \mu\text{m}$ . With  $\gamma_{\perp} = 2\pi \times 0.79 \text{ MHz}$  we obtain  $g = 2\pi \times 1.51 \text{ MHz}$ . The mirrors have high-reflectivity coatings with transmissions of 4 and 40 ppm, where the higher transmission side defines an output channel. From cavity decay measurements we infer a finesse of  $9 \times 10^4$  which yields a cavity lifetime of  $1.9 \mu\text{s}$  and a cavity decay rate  $\kappa = 2\pi \times 41.7 \text{ kHz}$ .

## 4. Theoretical model

To simulate the single-photon emission we use an eight-level model, including Zeeman sublevels of the ion and cavity Fock states as follows (see figure 3).

The system is initialized in the ground state  $|S_{1/2}, m_j = -1/2\rangle|0\rangle$  by optical pumping where we use the notation |atomic state, Zeeman sublevel> |cavity photon number>. A circularly polarized laser field with detuning  $\Delta_p$  couples this ground state to the state  $|P_{3/2}, m_j = -3/2\rangle|0\rangle$  with Rabi frequency  $\Omega$ . From the  $|P_{3/2}, m_j = -3/2\rangle|0\rangle$  state there are various spontaneous decay channels to the  $|S_{1/2}, m_j = -1/2\rangle|0\rangle$ ,  $|D_{3/2}, m_j = -3/2\rangle|0\rangle$  and  $|D_{3/2}, m_j = -1/2\rangle|0\rangle$  states with total decay rate  $\Gamma$  and to the  $|D_{5/2}, m_j = -1/2\rangle|0\rangle$ ,  $|D_{5/2}, m_j = -3/2\rangle|0\rangle$  and  $|D_{5/2}, m_j = -5/2\rangle|0\rangle$  levels with rate  $\gamma = (1 - \varepsilon)\gamma_{\parallel}$ , where  $\varepsilon$  denotes the solid angle covered by the cavity mode ( $\varepsilon \approx 10^{-4}$  for our cavity). The relative coupling strengths for the transitions from  $|P_{3/2}, m_j = -3/2\rangle|0\rangle$  to  $|D_{5/2}, m_j = -1/2\rangle|0\rangle$ ,  $|D_{5/2}, m_j = -3/2\rangle|0\rangle$  and  $|D_{5/2}, m_j = -5/2\rangle|0\rangle$  are  $1/\sqrt{10}$ ,  $\sqrt{2/5}$  and 1. If the ions ends up in the  $|D_{3/2}, m_j = -1/2\rangle|0\rangle$  or  $|D_{3/2}, m_j = -3/2\rangle|0\rangle$  states, it can be repumped to the ground state via the  $P_{1/2}$  state with a laser at 866 nm. All spontaneously emitted photons are considered as loss photons which can destroy the phase coherence between initial and final states. The ratio of spontaneously and stimulated emitted photons defines a quality factor for the transfer as discussed below.



All photons, which are scattered from the ion but not emitted into the cavity, are considered as *loss photons*. The loss rate is proportional to the population of  $P_{3/2}$  times the total spontaneous decay rate from this level.

## 5. Single-photon emission: theoretical results

### 5.1. Raman process

The Raman process is an effective two-level process, as discussed in section 2.1. The population of the intermediate state  $P_{3/2}$  can be kept very small by choosing large detunings  $\Delta_p$  and  $\Delta_c$ . The laser at 393 nm induces an AC-Stark shift of the level  $P_{3/2}$ . The Raman condition is satisfied if the cavity frequency is resonant with the transition from the  $|D_{5/2}, m_j = -5/2\rangle$  state to the  $|P_{3/2}, m_j = -3/2\rangle$  state, which is shifted by the AC-Stark effect. The effective Rabi frequency, which we call Raman–Rabi frequency, is  $\Omega_{RR} = g(\Omega/\Delta_p)$  and the effective emission rate can be calculated as  $\Gamma_{eff} = \Gamma_{sp} \Omega^2/(4\Delta_p^2)$ , where  $\Gamma_{sp} = \Gamma + \gamma_{\parallel}$  is the total emission rate from  $P_{3/2}$ .

The first condition for a Raman population transfer is  $\Omega_{RR} \gg \Gamma_{eff}$  such that unwanted spontaneous processes are suppressed. To fulfil this condition, it is important to note that  $\Omega_{RR}$  and  $\Gamma_{eff}$  can be altered by changing the ratio of  $\Omega/\Delta_p$  in a way such that  $\Omega_{RR} \gg \Gamma_{eff}$ . In this regime, one would expect Rabi oscillations if the two-photon resonance condition is fulfilled. Rabi oscillations can occur only when there is one photon in the cavity, which provides the energy to excite the ion. However, after the photon has been emitted from the cavity the ion remains in the state  $|D_{5/2}, m_j = -5/2\rangle|0\rangle$ .

As a second condition for phase-coherent transfer, the Raman–Rabi frequency has to be larger than the cavity decay rate  $2\kappa$  to achieve complete population transfer between states  $|S_{1/2}, m_j = -1/2\rangle$  and  $|D_{5/2}, m_j = -5/2\rangle$  before the photon leaves the cavity. The two conditions lead to the following boundaries for the ratio of  $\Omega/\Delta_p$ :  $\kappa/g < \Omega/\Delta_p < 4g/\Gamma_{sp}$ . With the numbers for  $g$  and  $\kappa$  given in section 3.2 and the total decay rate of the  $P_{3/2}$  state,  $\Gamma_{sp} = 2\pi \times 23$  MHz, we get  $0.027 < \Omega/\Delta_p < 0.26$ .

Figure 4 shows the time evolution of different level populations for three ratios of  $\Omega/\Delta_p$  under the assumption of an ideally coherent excitation (laser linewidth = 0). The effective Rabi frequency is equal to the cavity decay rate in the first case ( $\Omega/\Delta_p = 0.03$ ), whereas in the last case ( $\Omega/\Delta_p = 0.3$ ) it is comparable with the effective spontaneous decay rate. The Raman–Rabi oscillation is damped by the effective emission rate and by the cavity decay rate. Therefore, Rabi oscillations are hardly visible even though the system behaves as a two-level system.

Figure 5 shows the emission probability  $P_{em}$ , the photon emission time  $t_{em}$ , the quality factor  $\beta$ , all as defined in section 4, and the maximum population of the  $P_{3/2}$  state during the excitation process, as function of  $\Omega/\Delta_p$ . The emission probability  $P_{em}$  and the quality factor  $\beta$  are large for small values of  $\Omega/\Delta_p \ll 1$  as the population of the  $P_{3/2}$  state is kept small. The effective spontaneous emission rate is proportional to  $(\Omega/\Delta_p)^2$  and therefore decreases faster than the Raman–Rabi frequency, keeping the condition  $\Omega_{RR} > \Gamma_{eff}$  fulfilled. The width of the emitted photon pulse  $t_{em}$  increases with decreasing  $\Omega/\Delta_p$  as the Raman–Rabi frequency decreases. The photon emission probability  $P_{em}$  and the quality factor  $\beta$  reach a constant value for  $\Omega_{RR} \gg \Gamma_{eff}$ , i.e.  $\Omega/\Delta_p \ll 4g/\Gamma_{sp} = 0.26$  with our parameters. The Purcell factor  $\bar{F} = 1 + (2g^2)/(\kappa\Gamma_{sp})$ , which characterizes the enhancement of the photon emission into the cavity is  $\bar{F} = 5.86$  with our parameters. The spontaneous emission factor  $\beta'$ , i.e. the fraction of spontaneous emission

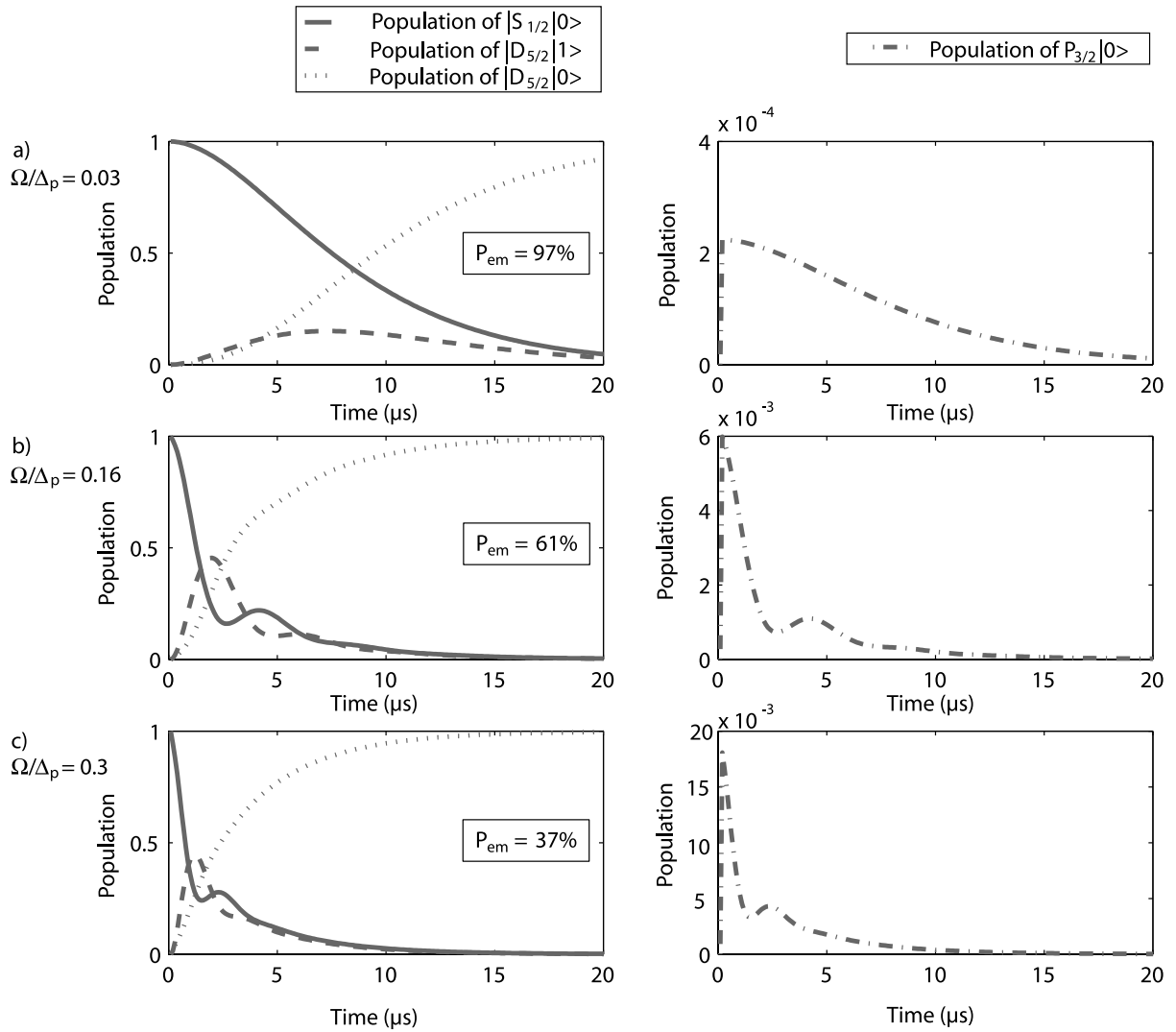


**Figure 4.** Time evolution of different level populations for the ideal Raman process. The ratio  $\Omega/\Delta_p$  is 0.03, 0.16, and 0.3 for (a), (b) and (c), respectively. The Raman–Rabi frequencies  $\Omega_{RR}$  are  $2\pi \times (0.045, 0.24, 0.45)$  MHz and the effective emission rates are  $\Gamma_{eff} = 2\pi \times (0.0048, 0.14, 0.48)$  MHz. The photon emission probability  $P_{em}$  is shown as inset for each configuration.

from the  $P_{3/2}$  level emitted into the resonant cavity mode, is  $\beta' = (\bar{F} - 1)/\bar{F} = 0.829$ . This value agrees well with the quality factor for the coherent population transfer  $\beta = 82.3\%$  obtained from the theoretical simulation for  $\Omega/\Delta_p \rightarrow 0$  (see figure 5).

If the Raman–Rabi frequency is smaller than the cavity decay rate,  $\Omega_{RR} < \kappa$  for  $\Omega/\Delta_p < 0.027$  with our parameters, the photon is emitted out of the cavity before it can be reabsorbed by the ion and no Rabi oscillation occurs (figure 4(a)). If, on the other hand, the ratio  $\Omega/\Delta_p$  increases, the Raman–Rabi frequency increases and becomes larger than  $\kappa$ . The emission time  $t_{em}$  now depends only on the cavity decay rate. The quality factor  $\beta$  decreases because the state  $P_{3/2}$  is increasingly populated and more photons are lost. Due to the increase of spontaneously emitted photons, the emission probability  $P_{em}$  decreases as well. If the ratio  $\Omega/\Delta_p > 0.26$ , the

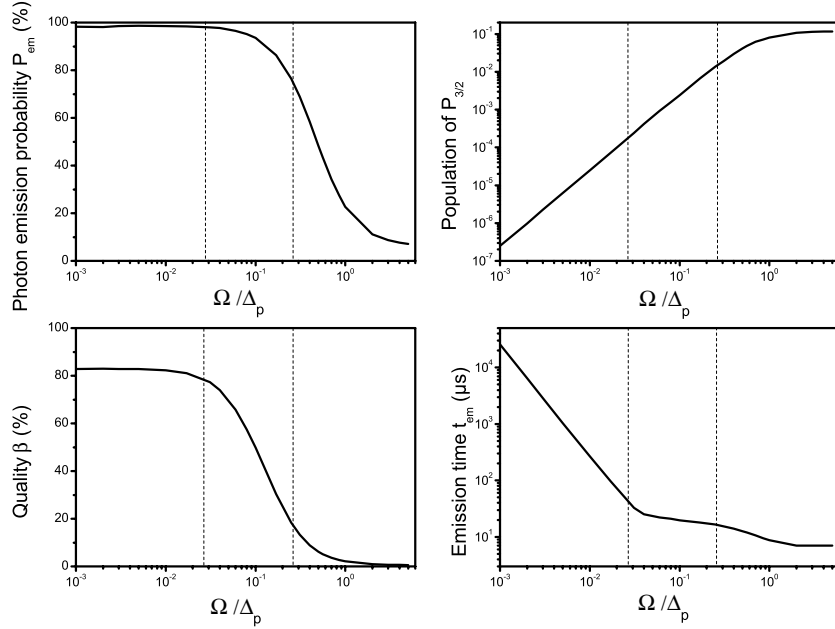


**Figure 5.** Emission probability  $P_{em}$ , photon emission time  $t_{em}$ , quality factor  $\beta$ , and maximum population of level  $P_{3/2}$  as a function of  $\Omega/\Delta_p$ . The parameters for the simulation are  $(\Omega, g, \kappa) = 2\pi \times (10, 1.5, 0.04)$  MHz. The dotted lines show the boundary conditions for  $\Omega/\Delta_p$  for fulfilling the conditions  $\Omega_{eff} \gg 2\kappa$  (left line) and  $\Omega_{eff} \gg \Gamma_{eff}$  (right line).

Raman–Rabi frequency  $\Omega_{RR}$  becomes smaller than the effective spontaneous emission rate  $\Gamma_{eff}$  and therefore the population transfer into the state  $D_{5/2}$  is small.

### 5.2. Adiabatic process

As discussed in section 2.2, the interaction of coherent light fields with a three-level system gives rise to new eigenstates (equation (2)). The energy splitting of these eigenstates is highest if the laser frequency and the cavity mode are near resonant with the specific atomic transition, i.e.  $\Omega, g \gg \Delta_c, \Delta_p$ . The adiabatic condition  $\dot{\theta} < |w^\pm - w^0|$  is thus achieved easiest for zero detuning which we accordingly have used in the following investigations. The dark state of our system is

$$|a^0\rangle = \cos\theta |S_{1/2}, m_j = -1/2\rangle |0\rangle - \sin\theta |D_{5/2}, m_j = -5/2\rangle |1\rangle \quad (5)$$

with the mixing angle  $\theta$  defined by  $\tan\theta = \Omega/(2g)$ .

A complete population transfer is possible only when the mixing angle is varied from 0 to  $\pi/2$ . To reach  $\theta = \pi/2$  it is necessary to turn the cavity coupling off. Experimentally, however, it is more appropriate to stabilize the cavity to one specific frequency instead of applying a time-dependent detuning. Nevertheless, a good population transfer is still possible if the Rabi frequency  $\Omega_0$  of the laser is much larger than the cavity coupling  $g$ . To give an example, for  $\Omega_0 = 6g(20g)$ , the final population of state  $|D_{5/2}, m_j = -5/2\rangle |1\rangle$  is 0.95 (0.995). Thus, we only vary the laser intensity for the simulation of the photon emission process. The pump laser Rabi frequency is modelled as  $\Omega(t) = \Omega_0 \sin^2(at)$  for  $0 < t < \tau$  and  $\Omega(t) = \Omega_0$  for  $t > \tau$  where

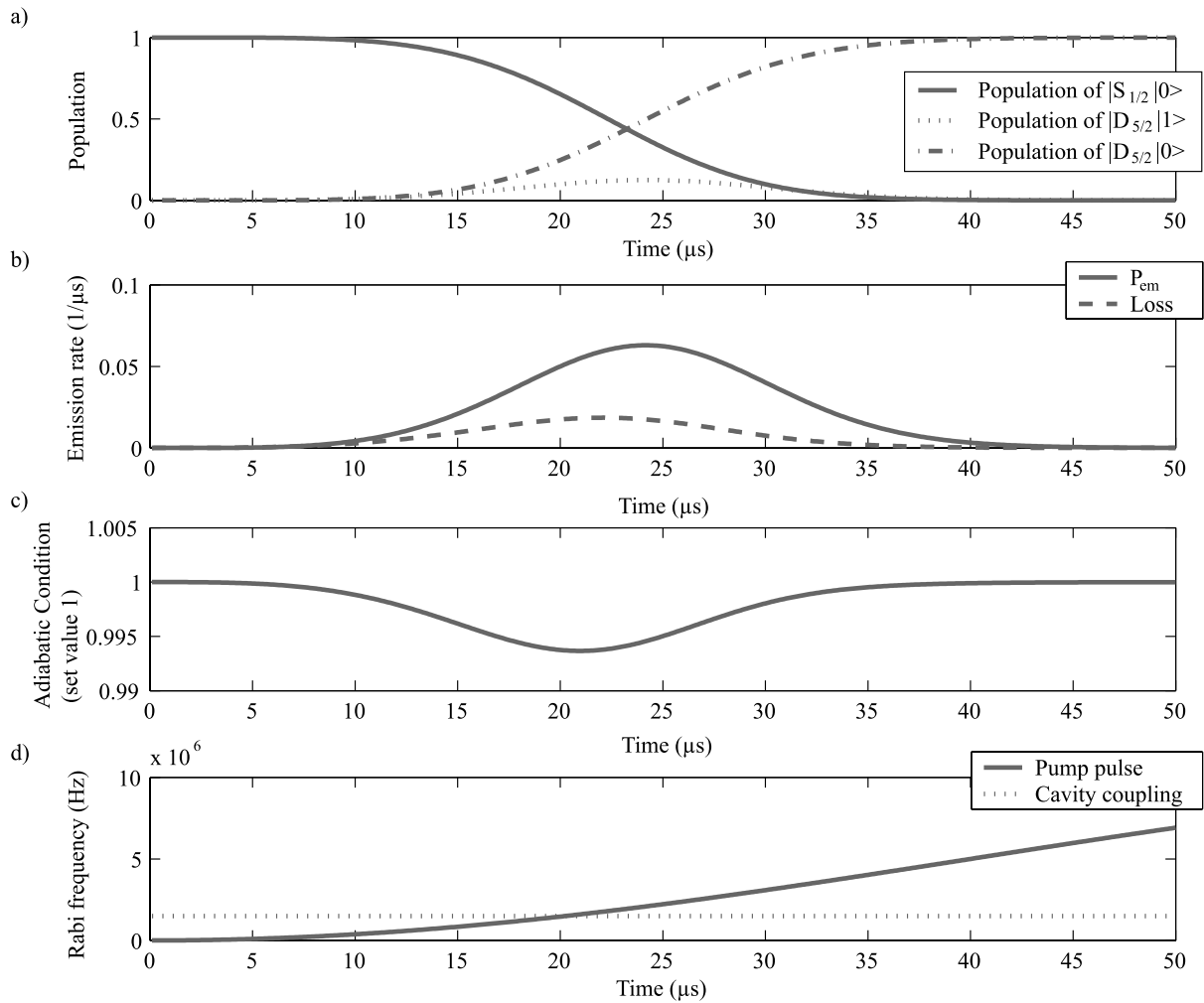


**Figure 6.** Time evolution of different level populations for the ideally coherent adiabatic process: (a) population of the three levels taking part in the adiabatic population transfer; (b) photon emission rate  $P_{em}$  and loss photon rate from state  $P_{3/2}$ ; (c) projection of the system onto the dark state  $a^0$ ; (d) time-varying pump pulse intensity and cavity coupling  $g$ . The cavity coupling  $g$  is kept constant. The parameters for the simulation are  $(\Omega_0, g, \kappa) = 2\pi \times (10, 1.5, 0.04)$  MHz, pulse rise time  $\tau = 80 \mu s$  and detunings  $\Delta_c = \Delta_p = 0$ .

$a = \pi/(2\tau)$  and  $\tau$  is the rise time of the pump laser pulse. To check the dependence of our results on the pulse shape, we also modelled the pump pulse as a Gaussian pulse or a linearly rising function.

Figure 6 shows a typical time evolution of an ideal lossless adiabatic process. The population is initially in the state  $|S_{1/2}, m_j = -1/2\rangle|0\rangle$  (solid line in figure 6(a)). By slowly increasing the laser intensity (solid line in figure 6(d)), the system follows the dark state and therefore the state  $|D_{5/2}, m_j = -5/2\rangle|1\rangle$  (dotted line in figure 6(a)) becomes populated. This state decays with the cavity decay rate  $2\kappa$  into the state  $|D_{5/2}, m_j = -5/2\rangle|0\rangle$  (dashed-dotted line in figure 6(a)). Figure 6(b) shows the emission rate for photons into the cavity  $P_{em}$  and the loss rate from level  $P_{3/2}$ . This level is populated due to an admixture of the  $P_{3/2}$  state to the dark state

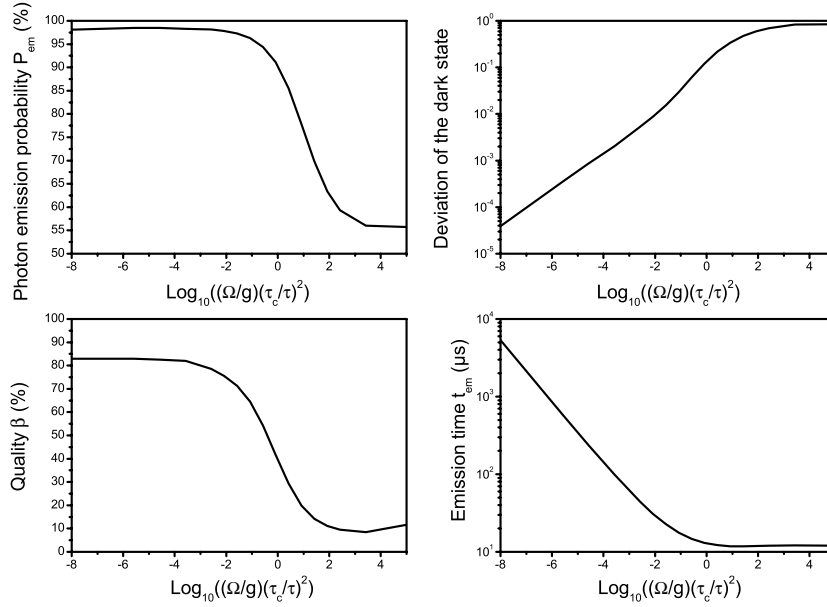


**Figure 7.** Emission probability  $P_{em}$ , photon emission time  $t_{em}$ , quality factor  $\beta$  and the deviation of the density matrix from the dark state  $1 - \langle a^0 | \rho | a^0 \rangle$  as a function of  $R = (\Omega_0/g) \times (\tau_c/\tau)^2$ . The parameters for the simulation are  $(\Omega_0, g, \kappa) = 2\pi \times (10, 1.5, 0.04)$  MHz.

by small deviations from adiabatic following and by damping of the system due to cavity decay and spontaneous emission. These deviations from the dark state can be monitored by calculating the projection of the system's density matrix onto the dark state  $a^0$  (figure 6(c)). Although the deviation is less than 1%, non-adiabatic following and damping leads to a significant loss rate. With the parameters given in figure 6, we yield an emission probability  $P_{em} = 97.9\%$ , an emission time  $t_{em} = 38.3 \mu\text{s}$  and a quality factor  $\beta = 77.7\%$ .

For further discussion we define the parameter  $R = (\Omega_0/g) \times (\tau_c/\tau)^2$  to characterize the adiabatic process, as we find that all processes with the same  $R$  lead to similar results. Here,  $\tau_c = 1/(2\kappa)$  is the photon lifetime in the cavity, and  $R$  correlates with Rabi frequency and rise time of the pump pulse with the respective cavity parameters. Figure 7 shows the emission probability  $P_{em}$ , the photon emission time  $t_{em}$ , the quality factor  $\beta$ , all as defined in section 4, and the deviation of the density matrix from the dark state  $1 - \langle a^0 | \rho | a^0 \rangle$  as a function of  $R$ . For large  $R$  the adiabatic condition is not fulfilled, and there are losses from the state  $P_{3/2}$  which is populated during the process. Here, the change of the laser intensity is too rapid for the system to follow the dark state. In case of a smaller  $R$ ,  $P_{em}$  and  $\beta$  reach a constant value. A further decrease of  $R$  leads to a slower population transfer and increasing photon pulse width  $t_{em}$ .

If the detunings  $\Delta_p$  and  $\Delta_c$  are increased, the process quality factor and photon emission probability stay unchanged as long as  $\Omega_0, g \gg \Delta_c, \Delta_p$ , i.e.  $\Delta_p = \Delta_c \ll 2\pi \times 10^6$ . Increasing the detunings further leads to reduced  $P_{em}$  and  $\beta$ .

### 5.3. Comparison of adiabatic and Raman process

Adiabatic and Raman processes can be seen as limiting cases of general coherent transfer schemes. Generally, a rapid adiabatic passage works best for small detunings from the atomic

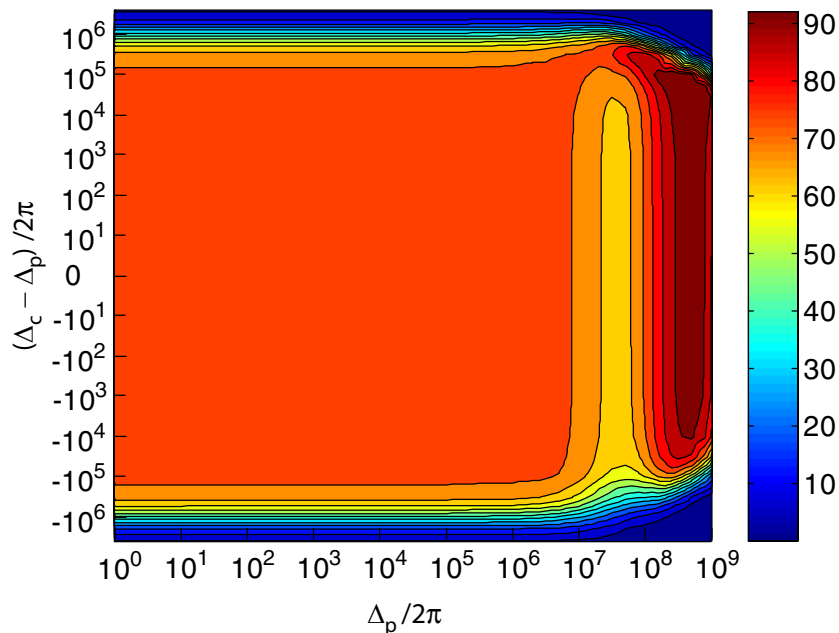


**Figure 8.** Photon emission probability  $P_{em}$  of a coherent transfer as a function of the pump laser detuning  $\Delta_p$  and of the relative detuning of pump laser and cavity  $\Delta_c - \Delta_p$ .  $\Delta_p$  is varied between 0 and  $2\pi \times (10^9)$  Hz, whereas  $\Delta_c$  is chosen such that the difference  $\Delta_c - \Delta_p$  varies between 0 and  $2\pi \times (6.7 \times 10^6)$  Hz. With this choice, we ensure that the adiabatic condition and the Raman condition can be exactly fulfilled for each pump laser detuning. The parameters for the simulation are  $\tau = 10 \mu\text{s}$  and  $(\Omega_0, g, \kappa) = 2\pi \times (10, 1.5, 0.04)$  MHz.

levels (section 5.2), whereas the Raman scheme requires large detunings (section 5.1). To monitor the transition from an adiabatic to a Raman passage, we calculate the photon emission probability of a coherent transfer as a function of pump laser and cavity detuning. In contrast with the model for the Raman passage, where the pump beam had a constant Rabi frequency, the pump pulse used here is modelled in the very same way as for the adiabatic passage described in the previous section, with a pulse rise time of  $\tau = 10 \mu\text{s}$ .

Figure 8 shows the photon emission probability  $P_{em}$  for different values of the pump laser and cavity detunings  $\Delta_p$  and  $\Delta_c$ . The photon emission probability  $P_{em}$  is plotted as a contour plot where blue areas indicate low probabilities and red areas indicate high probabilities. In the case of small detunings,  $\Delta_p < 2\pi \times (10^6)$  Hz and  $\Delta_c - \Delta_p < 2\pi \times (10^5)$  Hz, the condition for the adiabatic process is fulfilled and  $P_{em}$  reaches a value of  $\approx 76\%$  (bright red area in figure 8). Note that this value is smaller than the optimum value calculated in section 5.2 as the pump pulse rise time is slightly too short for the given value of  $\Omega_0$  and the system's state slightly deviates from the dark state (cf figure 7 with  $\log((\Omega_0/g) \times (\tau_c/\tau)^2) \approx 1$ ). A deviation from the two-photon resonance by less than  $2\pi \times (10^5)$  Hz does not change the efficiency of the adiabatic passage.

Increasing  $\Delta_p$  above  $2\pi \times (10^6)$  Hz initially leads to a reduction of  $P_{em}$  as the energy splitting between dark and bright states (equation (2)) becomes smaller and the dark state is no longer well-defined. If the pump laser detuning is much bigger than the pump laser Rabi frequency, i.e.  $\Delta_p > 2\pi \times (10^8)$  Hz in figure 8 (cf the case  $\Omega_0/\Delta < 0.1$  in figure 5), the system reaches the Raman regime (dark red stripe in figure 8). If the cavity is on Raman resonance,

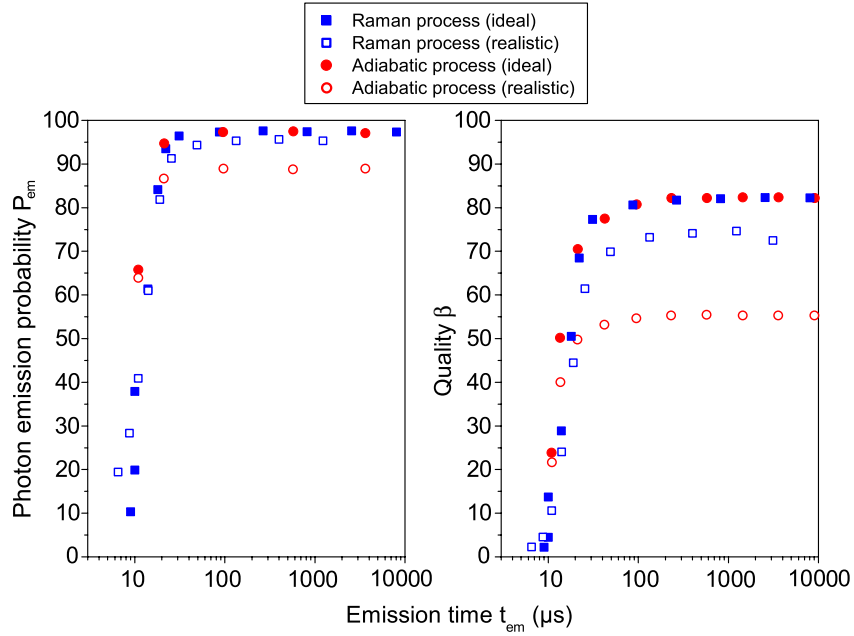


**Figure 9.** Photon emission probability  $P_{em}$  and quality factor  $\beta$  as a function of photon emission time  $t_{em}$  for the adiabatic process and the Raman process. The emission time  $t_{em}$  depends on  $R = \Omega_0/\tau^2$  for the adiabatic process and on the ratio  $\Omega/\Delta_p$  for the Raman process. Both ideal lossless (pump laser and cavity linewidth zero) and realistic lossy (pump laser and additional cavity linewidth of  $2\pi \times 10$  kHz, respectively,  $\delta_{ad} = \delta_{ram} = 2\pi \times 10$  kHz) processes are considered. The parameters for the simulation are  $\tau = 1$  s for the adiabatic process ( $\Omega_0$  is varied to cover the specified range of  $t_{em}$ ),  $\Omega = 2\pi \times 10$  MHz for the Raman process ( $\Delta_p$  is varied to yield the range of  $t_{em}$ ) and  $(g, \kappa) = 2\pi \times (1.5, 0.04)$  MHz.

i.e. the deviation of the cavity detuning  $\Delta_c$  from the Stark-shifted level  $\lambda_+$  is smaller than the cavity linewidth  $2\kappa$ , the photon emission probability is high ( $P_{em} \approx 94\%$ ).

A more realistic simulation of the photon emission process has to include the linewidth of the pump laser as well as the inhomogeneous linewidth of the frequency stabilized cavity [30] which may not be negligible compared with the homogeneous linewidth  $2\kappa$  due to jitter introduced by the frequency stabilization. Another source of experimental uncertainty is a deviation from the exact resonance conditions, i.e. a detuning of the cavity resonance from the AC-Stark shifted level  $\Delta_c \neq \lambda_+$  for the Raman process or a non-equal detuning  $\Delta_c \neq \Delta_p$  for the adiabatic process. We model these deviations by assuming  $\Delta_c - \lambda_+ = \delta_{ram}$  in the first case and by  $\Delta_c - \Delta_p = \delta_{ad}$  in the latter. Taking these linewidths and detunings into account, we obtain more realistic values for the photon emission probability  $P_{em}$  and the quality factor  $\beta$  of the two processes. The finite linewidths, however, have no effect on the photon emission time  $t_{em}$ . In figure 9, we compare the photon emission probability and the quality factor as a function of the emission time for the adiabatic process and the Raman process. For the modelling of the adiabatic process, we also used pump pulses with a Gaussian profile or linear slope. However, for identical photon emission times  $t_{em}$ , we find identical photon emission probabilities  $P_{em}$  for all pump pulse shapes.

For the ideal lossless case (zero pump laser and cavity linewidth), both the Raman and the adiabatic process provide very similar  $P_{em}$  and  $\beta$ . This behaviour changes when we include a

linewidth for the pump laser and the additional linewidth of the stabilized cavity of  $2\pi \times 10$  kHz. The photon emission probability  $P_{em}$  reduces by about 2% for the Raman process and by about 10% for the adiabatic process. The quality factor  $\beta$  for the processes is very sensitive to the considered linewidths and detunings.  $\beta$  is reduced by about 10% for the realistic Raman process and by about 30% for the realistic adiabatic process. For linewidths and detunings larger than  $2\pi \times 10$  kHz, both  $P_{em}$  and  $\beta$  decrease drastically. Thus, for realistic experimental parameters, the Raman scheme turns out to be more efficient.

## 6. Intensity correlation

In this section, we model the generation of a train of successive single photons. We consider the Raman process only since it is more efficient for realistic parameters, as shown in the previous section. The final state of the stimulated single-photon generation is the  $|D_{5/2}, m_j = -5/2\rangle|0\rangle$  state. If spontaneous emission from the  $|P_{3/2}, m_j = -3/2\rangle|0\rangle$  state occurred, the ion is found either in the  $|S_{1/2}, m_j = -1/2\rangle|0\rangle$  state or in one of the Zeeman sublevels of the  $|D_{5/2}, m_j = -5/2, -3/2, -1/2\rangle|0\rangle$  state. To bring the ion back into the initial ground state  $|S_{1/2}, m_j = -1/2\rangle|0\rangle$ , we apply a broad-band laser at 854 nm which excites the ion resonantly into the state  $P_{3/2}$ . This state decays with a branching ratio of 17.6 : 1 into the states  $S_{1/2}$  and  $D_{5/2}$ , respectively. Multiple excitation of the cavity mode due to spontaneous emission from the  $P_{3/2}$  state can be suppressed by detuning the cavity from the atomic resonance (which is inherently fulfilled for the Raman process). A circularly polarized laser at 397 nm finally pumps the ion to the  $|S_{1/2}, m_j = -1/2\rangle$  state.

In the theoretical model for the sequential generation of single photons, we use only the three ion states  $|S_{1/2}, m_j = -1/2\rangle$ ,  $|P_{3/2}, m_j = -3/2\rangle$  and  $|D_{5/2}, m_j = -5/2\rangle$  which are directly coupled by the population transfer processes. We also include the first three Fock states  $|n = 0\rangle$ ,  $|n = 1\rangle$  and  $|n = 2\rangle$  for the cavity mode. Therefore, we obtain the 9 levels depicted in figure 10. The lasers at 393 nm ( $\Omega_{393}$ ) and at 854 nm ( $\Omega_{854}$ ) couple levels of the same Fock state, whereas cavity coupling  $g$  and cavity decay  $\kappa$  increase (decrease) the Fock state by one. If the repump laser at 854 nm is applied too early it is possible to pump the ion into the state  $|S_{1/2}, m_j = -1/2\rangle|1\rangle$  with still one photon in the cavity. As a consequence there is a small probability to obtain a two-photon state in the cavity depending on the repetition rate of the whole photon generation and repumping sequence.

To quantify this two-photon probability we calculate the intensity correlation function  $g^2(\tau)$  defined as

$$g^2(\tau) = \frac{\langle a^\dagger(t)a^\dagger(t+\tau)a(t+\tau)a(t) \rangle}{\langle a^\dagger(t)a(t) \rangle \langle a^\dagger(t+\tau)a(t+\tau) \rangle}, \quad (6)$$

where  $a$  and  $a^\dagger$  are the photon annihilation and creation operators for the cavity mode, respectively. The correlation function  $g^2(\tau)$  is calculated using the quantum regression theorem [31]:

$$\begin{aligned} \langle a^\dagger(t)a^\dagger(t+\tau)a(t+\tau)a(t) \rangle &= \text{trace} \{ a^\dagger(t)a^\dagger(t+\tau)a(t+\tau)a(t)\rho(t) \} \\ &= \text{trace} \{ a^\dagger(t+\tau)a(t+\tau)\rho_i(t+\tau) \}, \end{aligned} \quad (7)$$

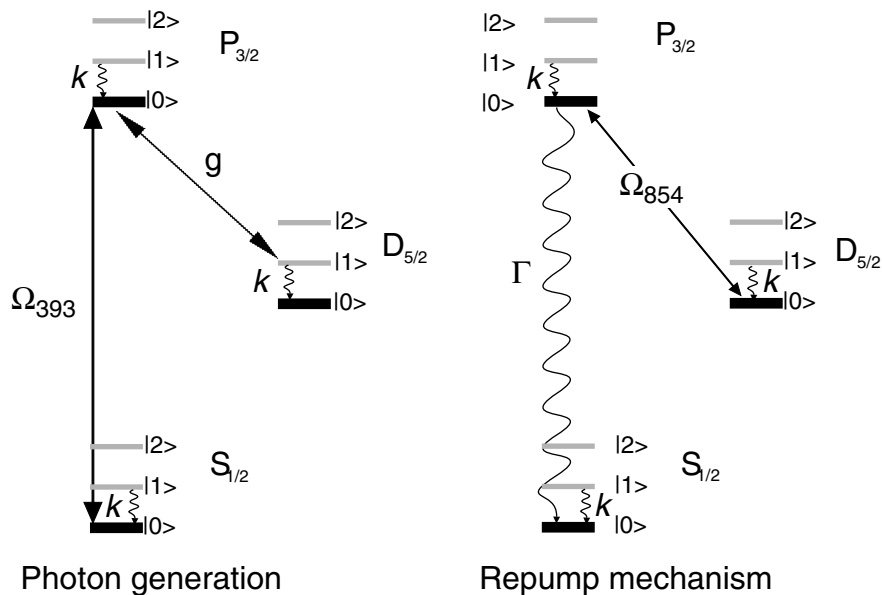


**Figure 10.** Nine-level model used for simulating sequential single-photon emission.

where  $\rho_t(t + \tau)$  denotes the density matrix evaluated at time  $t + \tau$  when the temporal evolution started with the density matrix  $\rho(t)$ , and the trace is calculated over all degrees of freedom. Figure 11 shows the time evolution of the considered ion states, the photon emission and the intensity correlation function for a sequence of four photon generation and repumping processes. The populations of the considered ion states (figure 11(a)) show the same time evolution as in figure 4. The emission of single-photon pulses into the cavity and the spontaneous decay from state  $P_{3/2}$  is plotted in figure 11(b). During the repeated sequences the cavity coupling  $g$  is always kept constant (figure 11(c)). The pump laser at 393 nm is turned off when the repump laser at 854 nm is applied to avoid excitation of cavity states with  $n > 1$ . The intensity correlation function  $g^2(\tau)$  is shown in figure 11(d). Note that the abscissa for the last diagram denotes the time delay between photon detection events, not an absolute time scale. The maxima of the intensity correlation function have the same spacing as the maxima of the emission rate into the cavity. For the parameters given above, we obtain  $g^2(0) < 10^{-4}$  for a photon pulse width of  $52 \mu\text{s}$  and a pulse repetition rate of  $1.9 \times 10^4 \text{ s}^{-1}$ .

## 7. Summary and discussion

We have presented theoretical calculations based on realistic parameters for deterministic single-photon generation from a single trapped ion. The comparison of adiabatic and pure Raman processes yields higher photon emission probabilities for the Raman process under assumption of realistic parameters. The probability  $P_{em}$  for emitting a single photon per pump pulse can be as much as 95% for the Raman process and up to 88% for the adiabatic process. Single-photon repetition rates of  $\approx 20 \text{ kHz}$  with vanishing two-photon probability  $g^2(0) < 10^{-4}$  are predicted. An experimental implementation of the single-photon emission scheme is currently in progress.

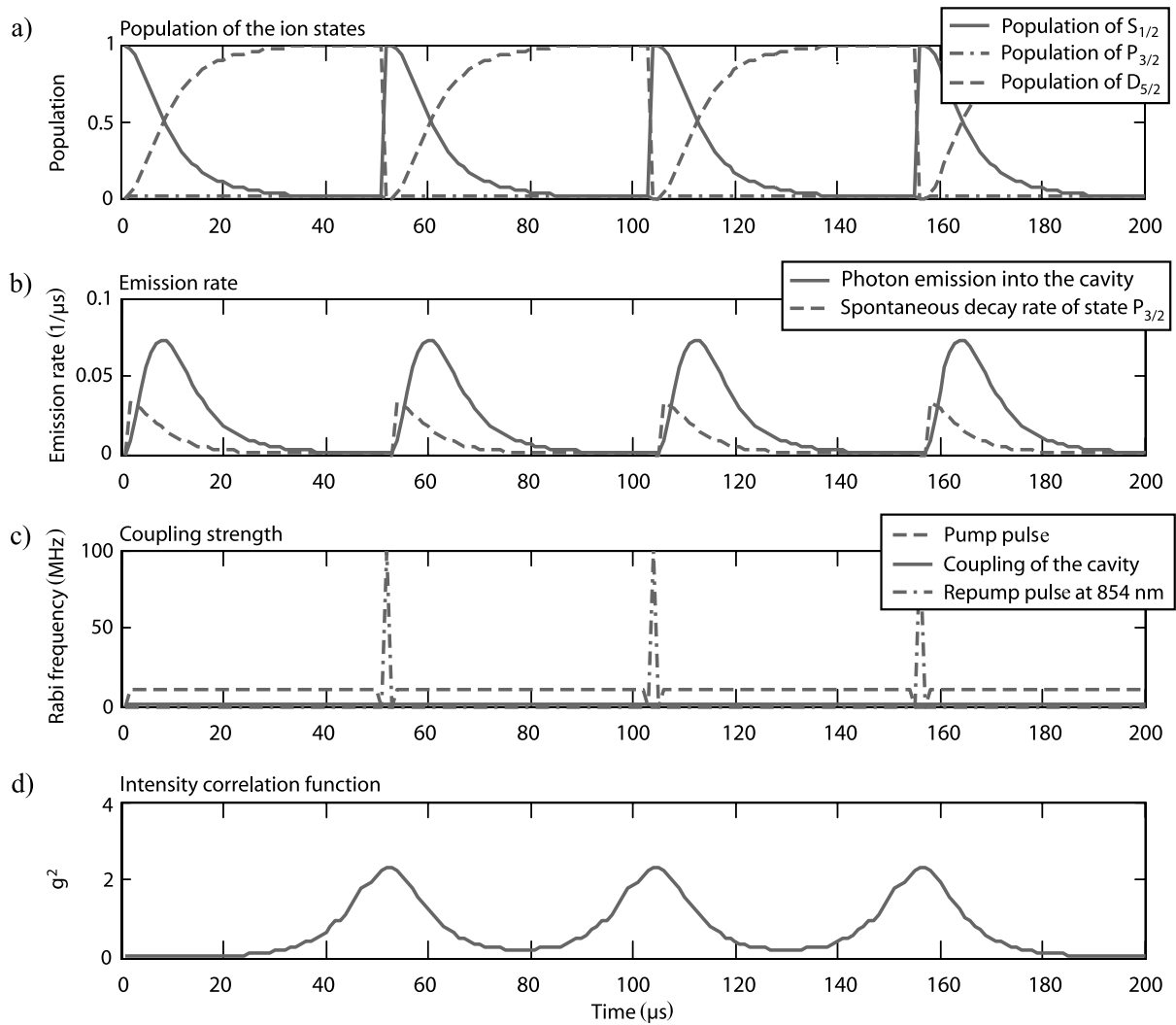


**Figure 11.** Time evolution of state populations, photon emission and intensity correlation function for a sequence of photon generation and repumping processes in the Raman scheme. Parameters for the simulation are  $(\Omega_{393}, g, \Delta_{393}, \kappa) = 2\pi \times (10, 1.5, 333, 0.04)$  MHz.

These numbers can be compared with recent realizations of single-photon sources with neutral atoms temporarily coupled to the mode of a high finesse cavity [12, 13]. In the first experiment [12], atoms are released from a magneto-optical trap and fall through the cavity in a way that the probability of finding a single atom inside the cavity at any given time is 5.7% (0.18% for 2 or more atoms). Each atom emits up to seven photons into the cavity mode with a repetition rate of 250 kHz. However, the average efficiency for single-photon emission into the cavity mode per excitation pulse is only 17% as the atoms are not localized at an antinode of the field, but have random trajectories. In the second experiment [13], on the other hand, atoms are stored in a dipole trap within the cavity mode volume for 0.14 s. Here, the measured emission probability per excitation pulse is consistent with unity and, on average, each atom emits  $1.4 \times 10^4$  photons during its storage time (repetition rate 100 kHz). In 3% of all storage

events two atoms are trapped which leads to  $g^2(0) \neq 0$  (16-fold suppression compared with a Poissonian light source). Again, atoms are not localized in the cavity standing wave and no number is given for the repetition rate of storage events.

A single-photon source based on a single trapped and localized ion, as proposed in this paper, would yield smaller repetition rates and longer pulses as the cavity coupling is weaker. Photon emission efficiencies would be comparable with the single stored atom source and exceed the efficiency of the ‘falling atom’ source. Its main advantage, however, would be the constant and predictable stream of triggered single photons, which can be emitted with defined polarization and can be extracted from the cavity with an efficiency of about 60%.

## Acknowledgments

We thank K Bergmann, M Hennrich, A Kiraz, G Morigi and H Ritsch for helpful discussions. This work is supported by the Austrian ‘Fonds zur Förderung der wissenschaftlichen Forschung’ (SFB15) by the European Commission IHP network ‘QUEST’ (HPRN-CT-2000-00121) and IST/FET program ‘QUBITS’ (IST-1999-13021) and by the ‘Institut für Quanteninformation GmbH’. C Russo acknowledges support by Fundação para a Ciência e a Tecnologia (Portugal) under the grant SFRH/BD/6208/2001.

## References

- [1] Bouwmeester D, Ekert A and Zeilinger A (ed) 2000 *The Physics of Quantum Information* (Berlin: Springer)
- [2] Brunel C, Lounis B, Tamarat P and Orrit M 1999 *Phys. Rev. Lett.* **83** 2722
- [3] Lounis B and Moerner W E 2000 *Nature* **407** 491
- [4] Kim J, Benson O, Kan H and Yamamoto Y 1999 *Nature* **397** 500
- [5] Kurtsiefer C, Mayer S, Zarda P and Weinfurter H 2000 *Phys. Rev. Lett.* **85** 290
- [6] Brouri R, Beveratos A, Poizat J-P and Grangier P 2000 *Opt. Lett.* **25** 1294
- [7] Michler P, Kiraz A, Becher C, Schoenfeld W V, Petroff P M, Zhang L, Hu E and Imamoglu A 2000 *Science* **290** 2282
- [8] Santori C, Pelton M, Solomon G, Dale Y and Yamamoto Y 2001 *Phys. Rev. Lett.* **86** 1502
- [9] Parkins A S, Marte P, Zoller P and Kimble H J 1993 *Phys. Rev. Lett.* **71** 3095
- [10] Law C K and Kimble H J 1997 *J. Mod. Opt.* **44** 2067
- [11] Kuhn A, Hennrich M, Bondo T and Rempe G 1999 *Appl. Phys. B* **69** 373
- [12] Kuhn A, Hennrich M and Rempe G 2002 *Phys. Rev. Lett.* **89** 067901
- [13] McKeever J, Boca A, Boozer D, Miller R, Buck J R, Kuzmich A and Kimble H J 2004 *Science* **303** 1992
- [14] Parkins A S, Marte P, Zoller P, Carnal O and Kimble H J 1995 *Phys. Rev. A* **51** 1578
- [15] Cirac J I, Zoller P, Kimble H J and Mabuchi H 1997 *Phys. Rev. Lett.* **78** 3221
- [16] Guthöhrlein G R, Keller M, Hayasaka K, Lange W and Walther H 2001 *Nature* **414** 49
- [17] Mundt A B, Kreuter A, Becher C, Leibfried D, Eschner J, Schmidt-Kaler F and Blatt R 2002 *Phys. Rev. Lett.* **89** 103001
- [18] McKeever J, Buck J R, Boozer A D, Kuzmich A, Nägerl H-C, Stamper-Kurn D M and Kimble H J 2003 *Phys. Rev. Lett.* **90** 133602
- [19] Sauer J A, Fortier K M, Chang M S, Hamley C D and Chapman M S 2003 *Preprint* quant-ph/0309052
- [20] Maunz P, Puppe T, Schuster I, Syassen N, Pinkse P W H and Rempe G 2004 *Nature* **428** 50
- [21] Roos C, Zeiger T, Rohde H, Nägerl H C, Eschner J, Leibfried D, Schmidt-Kaler F and Blatt R 1999 *Phys. Rev. Lett.* **83** 4713
- [22] Leibfried D, Blatt R, Monroe C and Wineland D 2003 *Rev. Mod. Phys.* **75** 281
- [23] Di Fidio C, Maniscalco S, Vogel W and Messina A 2002 *Phys. Rev. A* **65** 33825

- [24] Bergmann K, Theuer H and Shore B W 1998 *Rev. Mod. Phys.* **70** 1003
- [25] Gaubatz U, Rudecki P, Schiemann S and Bergmann K 1990 *J. Chem. Phys.* **92** 5363
- [26] Liaw S 1995 *Phys. Rev. A* **51** 1723
- [27] Schmidt-Kaler F *et al* 2003 *Appl. Phys. B* **77** 789
- [28] James D F V 1998 *Appl. Phys. B* **66** 181
- [29] Gardiner C W and Zoller P 2000 *Quantum Noise* (Berlin: Springer)
- [30] Mundt A B, Kreuter A, Russo C, Becher C, Leibfried D, Eschner J, Schmidt-Kaler F and Blatt R 2003 *Appl. Phys. B* **76** 117
- [31] Carmichael H J 1999 *Statistical Methods in Quantum Optics 1* (Berlin: Springer)